ACS NANO
Cite This: ACS Nano XXXX, XXX, XXX−XXX
www.acsnano.org

ARTICLE

Piezoelectric Effect Tuning on ZnO Microwire Whispering-Gallery Mode Lasing

Junfeng Lu,[†,‡] Chunxiang Xu,[*,§] Fangtao Li,[†] Zheng Yang,[†,‡] Yiyao Peng,[†,‡] Xiaoyi Li,[†] Miaoling Que,[†,‡] Caofeng Pan,[*,†,‡] and Zhong Lin Wang[*,†,‡,∥]

[†]Beijing Institute of Nanoenergy and Nanosystems, Chinese Academy of Sciences, Beijing 100083, P. R. China
[‡]College of Nanoscience and Technology, University of Chinese Academy of Sciences, Beijing 100049, P. R. China
[§]State Key Laboratory of Bioelectronics, School of Biological Science and Medical Engineering, Southeast University, Nanjing 210096, P. R. China
[∥]School of Materials Science and Engineering, Georgia Institute of Technology, Atlanta, Georgia 30332-0245, United States

S *Supporting Information*

ABSTRACT: **We report a dynamic tuning on coherent light emission wavelengths of single ZnO microwire by using the piezoelectric effect. Owing to the dominant role occupied by the piezoelectric polarization effect in the wurtzite-structure ZnO microwire, the effective dielectric constant (or refraction index) of the gain media was modulated toward an increasing trend by applying a tensile strain, resulting in a shift of the strain-mediated whispering-gallery mode (WGM) lasing at room temperature. Also, the strain required to resolve the spectra in the two operating types of PL and lasing were systematically analyzed and compared. Because of the narrow line width in the lasing mode, the strain-dependent spectral resolution was improved by an order of magnitude, making it feasible for achieving high-precision, ultrasensitive, and noncontact stress sensing. Our results have an important impact on laser modulation, optical communication, and optical sensing technology.**

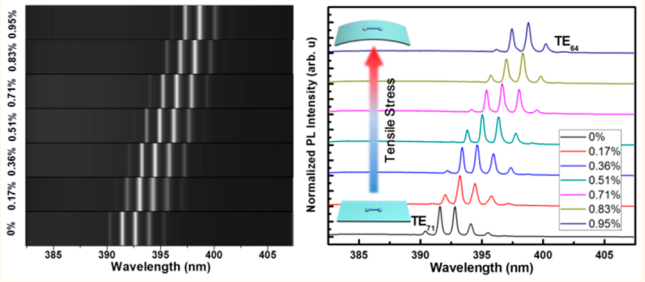

KEYWORDS: *whispering gallery mode, ZnO, microlasers, piezoelectric effect, strain sensor*

Lasers have huge applications in science and technology, from medical to manufacture and to defense. An important characteristic of a laser is its wavelength and width of wavelengths. Various approaches, including bandgap engineering,[1−4] self-absorption effect,[5,6] and Burstein−Moss (BM) effect,[7] have been developed for tuning the lasing modes of a solid-state device. Wavelength tunable nanolasers are promising for multifunctional applications in all-optical integrated nanodevices, optical communication, optical sensing technology, and spectroscopy analysis.[8,9] However, all of these methods mentioned above for tuning the lasing modes lack a dynamical tenability, that is, the ability to reversibly modulate the stimulated emission in a preprepared single micro- and nanodevices. Therefore, it is extremely urgent to develop an approach for tuning the coherent light emission dynamically.

In 2007 and 2010, two original concepts of piezotronics and piezophototronics were proposed by Wang and co-workers[10−13] based on the three-field coupling among semiconductor, photoexcitation, and piezoelectricity in wurtzite-structural semiconductors under mechanical perturbations. It is expected to tune the lasing modes by the tunable refractive index caused by the piezoelectric polarization effect in wurtzite-structural semiconductors by applying a strain. The wurtzite-structural ZnO, due to its characteristics of wide direct bandgap (3.37 eV) and high exciton binding energy (60 meV), has been considered as a promising material for applications in photodetectors,[14−16] UV laser devices,[17−20] and piezoelectric devices.[21−23] Particularly, some major advances in ZnO micro/nanostructures based functional devices have been achieved by utilizing its piezoelectricity such as stress sensing devices,[24,25] flexible optoelectronic devices,[26,27] and nanogenerators.[28,29] In addition, early researches reported the existence of piezoresistive effect in ZnO and other wurtzite-structural semiconductor materials.[30] The optical bandgap of ZnO can be effectively tuned by external mechanical compressive and tensile strain.[31−33] The variation in optical bandgap is linearly related to the applied stress, allowing us to observe the shift of NBE emission peak to determine the magnitude of the applied stress. In contrast, although the

Received: August 26, 2018
Accepted: November 8, 2018
Published: November 8, 2018

DOI: 10.1021/acsnano.8b06500
ACS Nano XXXX, XXX, XXX−XXX

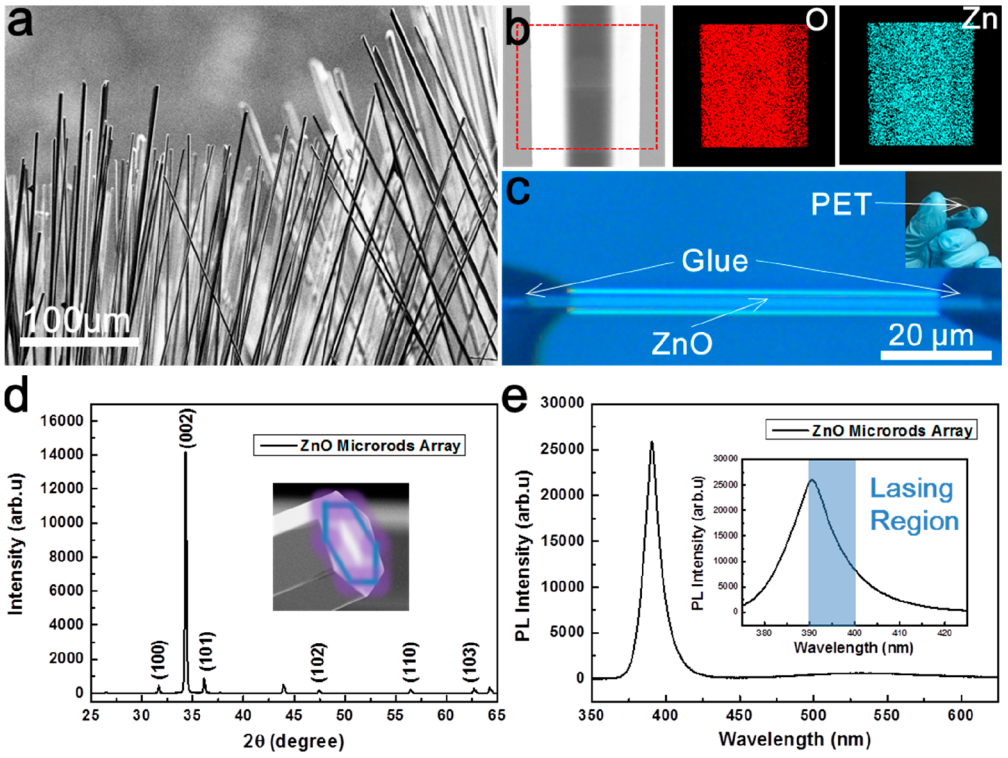

Figure 1. Morphology, structural characterization and optical performance of ZnO microwire. (a) SEM image of ZnO microwire arrays. (b) Zn and O element mapping. (c) Optical image of single ZnO microwire fixed on the flexible PET substrate; inset, optical image of PET. (d) XRD pattern of ZnO microwire arrays inserted with an enlarged SEM image of single ZnO microwire cross-section. (e) PL spectrum of ZnO microwire arrays; inset shows the lasing region.

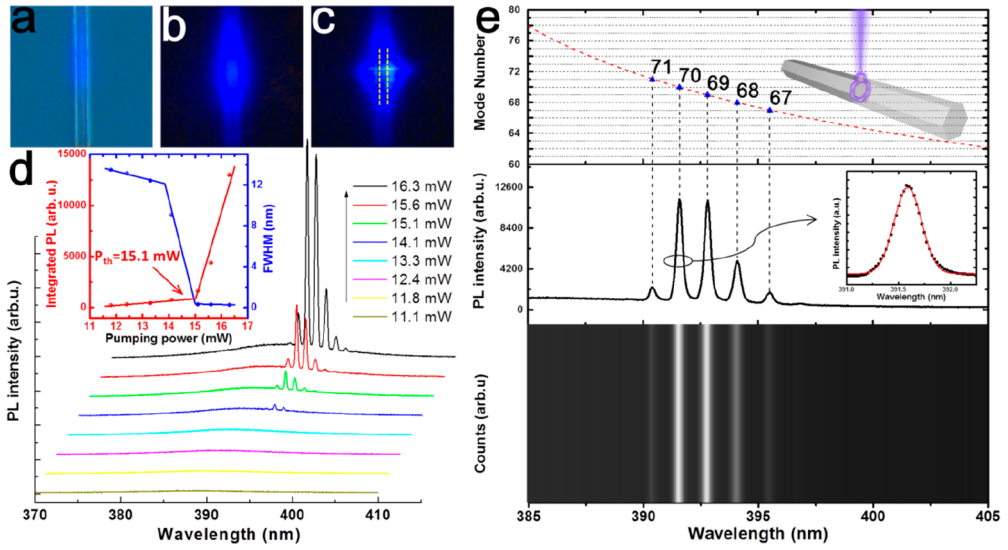

Figure 2. Lasing characteristics and mode analysis. Bright-field (a), dark-field optical images of an individual ZnO microwire below (b) and above (c) lasing threshold. (d) Power-dependent lasing spectra of the measured ZnO microwire; inset, dependence of the integrated lasing intensity and fwhm on pumping power. (e) Spectrum (middle panel) and mapping (below panel) of lasing emission excited at 15.6 mW. The relationship between the simulated TE mode numbers (blue triangle) and peak positions (black dash line), Insets show the schematic diagram of the WGM in ZnO microcavity and the magnification of one lasing peak by Gaussian fitting.

fluorescence signal based stress sensors have the advantages of convenience and intuitiveness, some critical shortcomings, including low accuracy and wide spectral range, limit its applications in practice. Therefore, design and development of high-sensitivity, high-precision, and noncontact stress sensing components are the major goals for researchers.

Here, combined with high exciton binding energy and excellent piezoelectric properties of ZnO, we have developed an approach to detect the applying stress through the WGM lasing mode evolution. Utilizing the piezoelectric polarization effect of ZnO, the lasing modes have been modulated effectively because of the increased refractive index under the tensile strain. Compared with the PL-type operation, the lasing

DOI: 10.1021/acsnano.8b06500
ACS Nano XXXX, XXX, XXX−XXX

peaks can be resolved at a lower order of magnitude applied tensile strain because the line width of the lasing modes is much smaller than the bandwidth of ZnO NBE emission. The lasing-type operated strain sensors exhibit the advantages of high precision, high resolution, and noncontact. It indicates that this concept of strain-mediated WGM lasing mode shift might enforce studying on strain sensing and optical signal modulation.

RESULTS AND DISCUSSION

Figure 1a shows the scanning electron microscope (SEM) image of ZnO microwire arrays grown on silicon substrate with a diameter ranging from 1 to 20 μm. The length of the prepared ZnO microwires can reach up to a few millimeters or even one centimeter. The element mapping images collected from the red rectangle region in Figure 1b indicate that Zn and O elements are uniformly distributed distinctly along to the profile of ZnO microwire. To examine the crystalline quality, a typical XRD pattern of ZnO microwire arrays is shown in Figure 1d, from which it can be seen that all of the diffraction peaks of the sample match well with the indexes of the wurtzite phase of ZnO (JCPDS no. 36-1451) with lattice constants of a = 3.250 Å and c = 5.207 Å. The strong and narrow diffraction peak at $2\theta = 34.32°$ are peculiar to the (002) plane of wurtzite ZnO, with a hexagonal cross section shown in the inset of Figure 1d, which indicates that the ZnO microwires with high crystallinity mainly grow along the [0001] direction. The high crystalline hexagonal structure provides a natural configuration, where the light can propagate circularly in the cavity due to multiple total internal reflections at the inner walls and reduce energy loss. It is expected to obtain a high Q factor and low threshold WGM lasing from this cavity. In addition, ZnO is also an excellent optical gain medium. As shown in Figure 1e, a strong intrinsic NBE emission peak at 390 nm and a weak defect-related emission peak at 530 nm can be observed which will afford sufficient optical gain for lasing mainly occurred in the highlighted region of Figure1e's inset. To apply the tensile strain on an individual ZnO microwire, it was placed on the flexible polyethylene terephthalate (PET) substrate and fixed by a kind of epoxy resin glue (A/B) to avoid the slippage during the bending process, as shown in Figure 1c.

To examine the optical performance of the ZnO microcavity, the lasing spectra was measured by utilizing a confocal μ-PL system coupled with a focused nanosecond pulsed laser operating at 355 nm as the excitation source at room temperature. Figure 2d shows the power-dependent lasing spectra of an individual ZnO microwire. At a low pumping power of 11.1 mW, where a weak and broad spontaneous emission located at around 390 nm can be observed, the full width at half-maximum (fwhm) is about 13 nm. When the pumping power is increased to 14.1 mW, two discrete peaks emerge from the broad spontaneous emission. When the pumping power is further increased to 16.3 mW above threshold, more lasing peaks are obtained with the fwhm of ~0.3 nm. According to $Q = \lambda/\Delta\lambda$, where λ and $\Delta\lambda$ are the wavelength and fwhm of the lasing peak, respectively. Thus, the Q factor of this microcavity can be estimated to about 1300. The inset of Figure 2d presents the integrated PL intensity and fwhm as a function of the pumping power. When the pumping power is below the threshold (15.1 mW), PL intensity increases slowly with a wide fwhm. As the pumping power is above the threshold, PL intensity increases dramatically with a narrow fwhm. It indicates the transition from spontaneous emission to stimulated emission and appearance of the nonlinear lasing phenomena. Figure 2a–c shows the optical images of ZnO microcavity excited by a focused laser. It is worth noting that above threshold, ZnO microcavity emitted more dazzling blue-violet lasing with some clear interference fringes from the edge positions highlighted by a yellow dash line compared with the one below threshold. This predicts the resonant process may come from a WGM cavity provided by ZnO microwire.

To further confirm the resonant process of this cavity, the lasing characteristics were analyzed, as shown in Figure 2e. Generally, the output lasing involves both TE and TM polarization. However, only TE mode is observed in our case because TM polarized emission is much weaker than the corresponding TE mode.[34,35] Therefore, we just discuss the lasing behavior of TE mode here. The refractive index of TE mode can be described by the Sellmeier's dispersion function,[36]

$$n(\lambda) = \left(1 + \frac{2.4885\lambda^2}{\lambda^2 - 102.30^2} + \frac{0.215\lambda^2}{\lambda^2 - 372.60^2} + \frac{0.2550\lambda^2}{\lambda^2 - 1850^2}\right)^{1/2} \quad (1)$$

The mode number N and corresponding resonant wavelength λ can be deduced by a plane wave model for hexagonal WGM cavity,[37,38]

$$N = \frac{3\sqrt{3}nD}{2\lambda} - \frac{6}{\pi}\tan^{-1}\left(n\sqrt{3n^2 - 4}\right) \quad (2)$$

where D is the diameter of cavity and n is wavelength-dependent refractive index. Figure 2e shows the spectrum and corresponding mapping of lasing emission under the pumping power of 15.6 mW. The calculated WGM TE mode numbers from 67 to 71 are plotted as blue triangles. The experimental resonant wavelengths that match with the theoretical modes very well are listed in Table 1. Therefore, it is confirmed that the lasing behavior here is due to WGM.

Table 1. Theoretical, Experimental Resonant Wavelength, and Calculated TE Mode Number

	N (mode no.)				
	71	70	69	68	67
theory	390.40	391.58	392.77	394.07	395.51
experiment	390.41	391.59	392.81	394.10	395.52

As schematically shown in Figure 3a, a tensile strain was applied on an individual ZnO microcavity by bending the flexible PET substrate operated through two 3D manual stages. Simultaneously, they also can be used to refocus the incident light on the ZnO microwire in the process of applying stress. To illustrate that the uniaxial tensile stress was applied, Raman spectra under different strain was measured (see Figure S2 in Supporting Information). It is noted that the E_{2L}, second-order, E_{1TO}, and E_{2H} phonon frequencies downward shift with increasing tensile strain up to 0.76%, while the A_{1TO} peak has no obvious change and keeps at the original positions when the tensile strain is applied. This experimental phenomenon is quite different from the previous results observed through a hydrostatic pressure test on bulk ZnO crystal,[40,41] which is caused by the different strain loading methods. The former is the uniaxial tensile strain along the c-axis and leading to elongation of the lattice, while the latter is an isotropic strain

DOI: 10.1021/acsnano.8b06500
ACS Nano XXXX, XXX, XXX–XXX

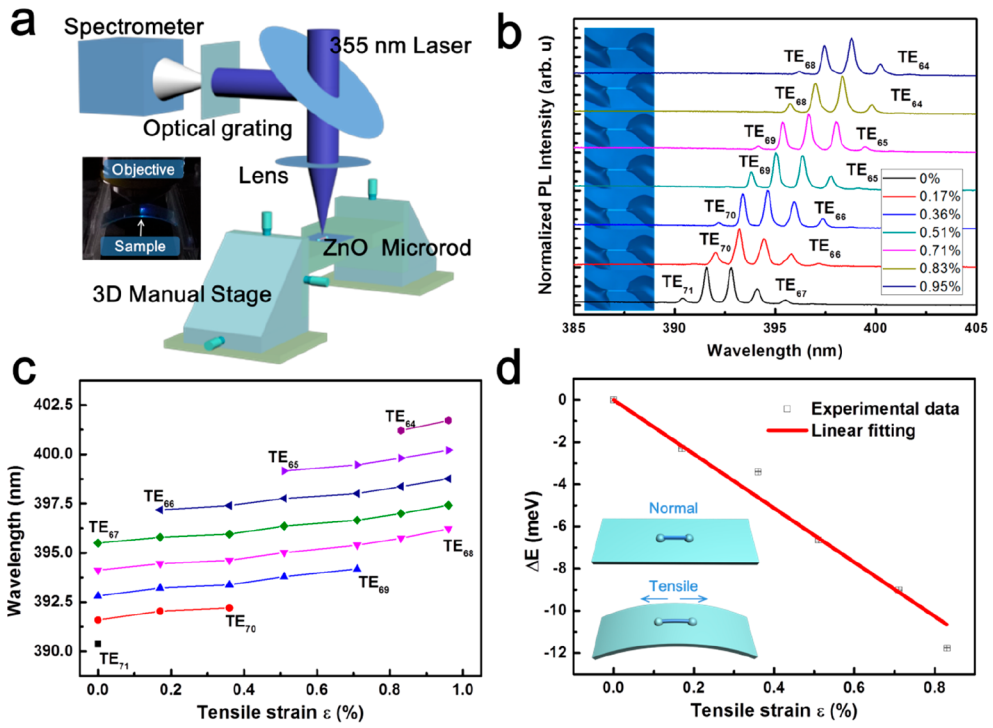

Figure 3. Lasing spectra under tensile strain. (a) Schematic diagram of PL measurements for single ZnO microwire fixed on a flexible PET substrate under the tensile strain controlled by 3D manual stage. (b) Lasing spectra of ZnO microcavity under different degrees of bending inserted with optical images of the sample. (c) The relationship of different TE modes with the applying tensile strain. (d) Dependence of the mode-shift on the applied tensile strain.

under the hydrostatic pressure on the ZnO crystal and resulting in isotropic compression of the lattice. The inset in Figure 3a shows the real optical picture of the bending sample under the excitation laser of 355 nm focused by an objective lens integrated on an upright microscope. By controlling the relative distance between the two 3D manual stages, the lasing spectra collected from the same sample under different degrees of bending can be obtained, as shown in Figure 3b. With increasing of tensile strain, the phenomena of redshift for the lasing peaks accompanied by the modes appearance and disappearance can be observed obviously. Comparing the measured spectra, the total amount of shifting is larger than the mode space (Free spectral range, FSR). In contrast, the blueshift of the lasing mode was observed by Chen et al.[39] from organic dye molecules (R6G) doped polymer microfibers under the tensile strain. They deemed that the lasing mode shift can be ascribed to the decreased refractive index because of the "dilute" polymer and PDMS by applying the tensile strain. However, the situation is completely different in our case. First, the ZnO microwire in the excited region is exposed to air with the unchanged refractive index during the bending. Second, for the wurtzite ZnO, the polarizability of the ions play a greater effect on the refractive index compared with the decreased number of dispersion centers per unit volume.[42] According to the Poisson ratio of ZnO (~0.35), the variation of D can be estimated as 3.57, 7.56, 10.71, 14.91, 17.43, and 19.95 nm under the tensile strain of 0.17%, 0.36%, 0.51%, 0.71%. 0.83%, and 0.95%, respectively. If we only consider the change of the cavity, the mode wavelength can be calculated as shown in Supporting Information, Table S1. A slight blueshift can be observed, which is contrary to the experimental results. Thus, the redshift of lasing mode in this work can be attributed to the increased refractive index due to the polarization under the tensile strain. Figure 3c plots the dependence of the entire arisen mode positions on the applying tensile strain. During the bending, some high-order modes at the short-wave side disappear, while some lower-order modes at long-wave side emerge. All the mode positions exhibit the same trend as the applied tensile strain increases. Further analysis of TE_{67} mode photon energy redshift versus the applied tensile strain is plotted in Figure 3d. The photon energy of redshift increases linearly with the increased tensile strain.

To further investigate the characteristics of the strain-sensitive WGM lasing, the spontaneous emission of the ZnO microwire was measured and used to compare with the stimulated emission. Figure 4a demonstrates the PL spectra of ZnO microwire under different tensile strain ranging from 0% to 0.90%. As the applied tensile strain increases, an obvious redshift of NBE emission peak changing from 388.44 to 393.54 nm was observed. Figure 4b compares the redshift variation for the NBE emission and lasing mode photon energy as a function of the tensile strain value. It can be seen that the photon energy redshift (ΔE) of the spontaneous emission is greater than that of the stimulated emission, which suggested the essential difference of the underlying mechanisms leading to the spectral evolution. The former is attributed to the variation of the strain-induced energy bandgap shown in sketch of Figure 4e, while the latter is ascribed to the increasing of the refractive index caused by the polarization effect under the tensile strain as mentioned before. The linear relationship between the energy redshift ΔE and the tensile strain ε can be expressed as $\Delta E = k\varepsilon$, where $k = \partial E/\partial \varepsilon$ is the deformation potential. Through the linear fitting of the plotted data (black square) in Figure 4b, the bandgap deformation potential $k = -41$ meV/% can be obtained, which is similar to the previous reports.[40] To more clearly observe the redshift phenomenon

DOI: 10.1021/acsnano.8b06500
ACS Nano XXXX, XXX, XXX−XXX

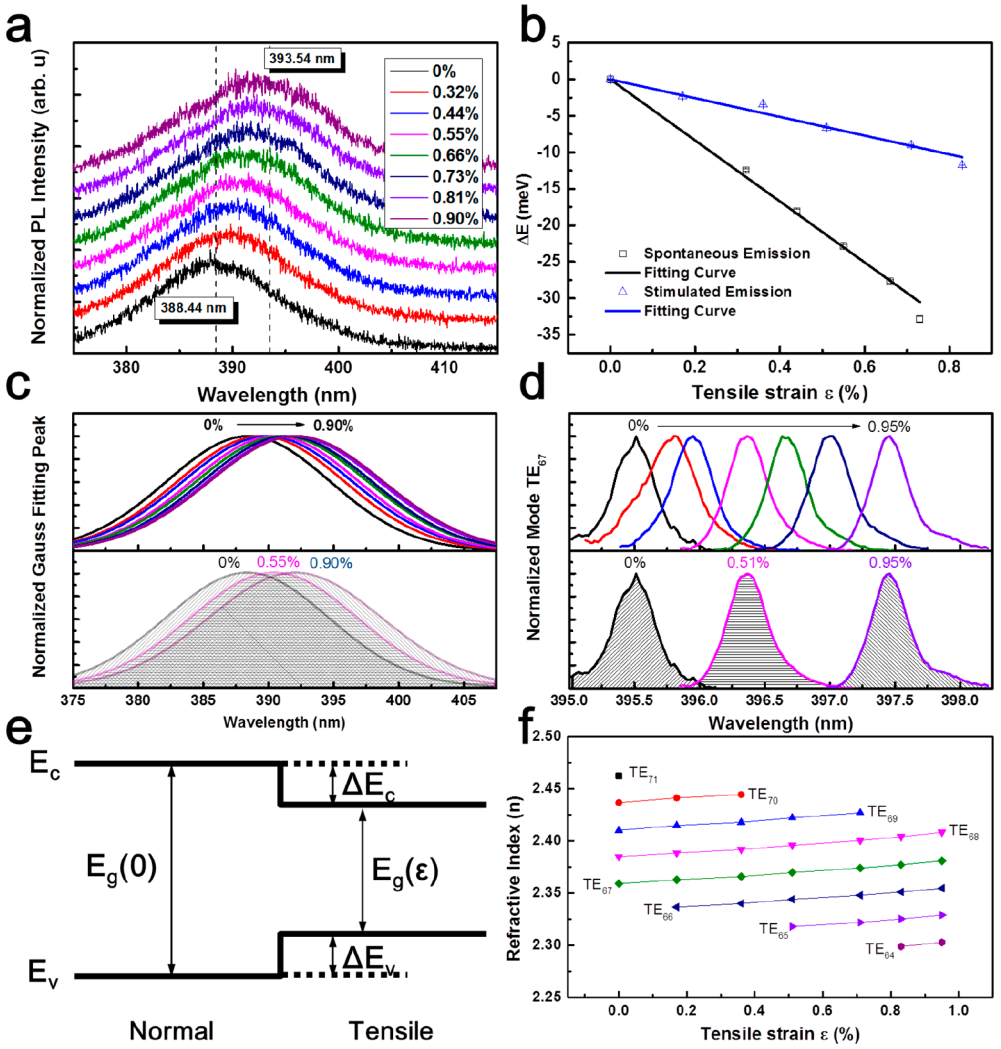

Figure 4. redshift of PL spectra under tensile strain in comparison to lasing mode shift. (a) PL spectra of ZnO microcavity under different degrees of bending. (b) Comparison of the redshift variation for the NBE emission and lasing mode photon energy as a function of the tensile strain value. (c) Normalized Gaussian fitting of PL spectra and (d) Normalized mode TE_{67} under different degrees of bending. (e) Schematic diagram of energy bandgap shift under normal and tensile states. (f) The refractive index of different lasing modes as a function of the tensile strain.

caused by tensile strain, the NBE emission peaks under different degrees of bending were fitted by Gaussian function (see Figure S4 in Supporting Information). All of the fitting curves are matched well with the experimental data with the *R*-square greater than 0.97. On the other hand, the strain-induced polarization field may affect the free excitons of semiconductor materials at room temperature, thus causing the intensity of NBE emission to change, further affecting the medium gain. However, the effect of the piezoelectric polarization field is not obvious because the binding energy (60 meV) of the exciton in ZnO is much larger than the thermal ionization energy (26 meV) at room temperature. Figure 4f plots the refractive index of different lasing mode as a function of the applied tensile strain. For the same lasing mode, the refractive index will increase with increasing of the applied tensile stress, accompanied by the redshift of lasing mode wavelength (see Figure S5 in Supporting Information). The slope of the linear fitting curve for the high-order mode is larger than that of the low-order mode, implying the greater impact of the piezoelectric effect on the refractive index at the resonant frequency closed to the bandgap energy. Parts c and d of Figure 4 compare the normalized Gaussian fitting of PL spectra and lasing mode TE_{67} under different degrees of bending. Obviously, the spectral resolution of lasing mode operated by tensile strain is higher than that of the energy band-mediated PL spectra. When the tensile strain increases to 0.90%, most area of PL spectra is still overlapped with that under tensile strain of 0%. Surprisingly, the lasing modes shown in Figure 4d are completely separated from each other as the tensile strain increases to 0.51%. More intuitive distinction can be observed in the mapping of lasing mode and NBE emission applying with different degrees of bending (see Figure S3 in Supporting Information). This concept of dynamically tunable lasing mode provides an effective approach for developing the high-precision, ultrasensitive, and noncontact strain sensors.

To verify the ability to regulate the lasing mode by applying external mechanical strain, we further carried out strain-mediated lasing measurement on two other ZnO microwires with different diameters of 5.89 and 4.02 μm, which were named as #1 and #2, respectively. Figure 5a shows the lasing spectra of ZnO microwire with a diameter of 5.89 μm under

DOI: 10.1021/acsnano.8b06500
ACS Nano XXXX, XXX, XXX−XXX

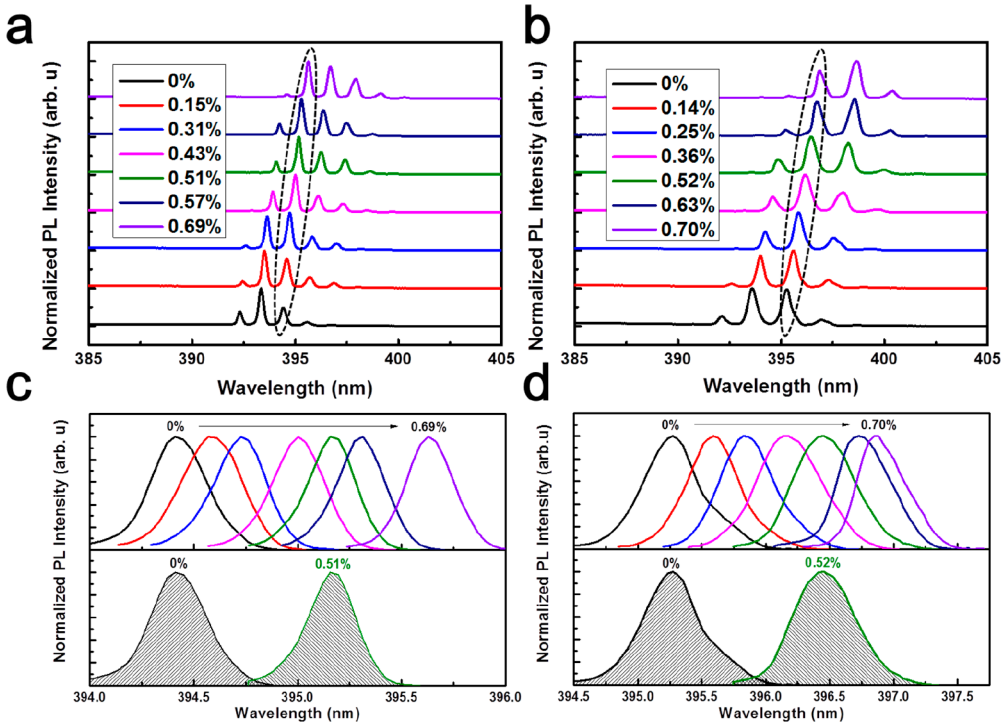

Figure 5. Repeatability and reproducibility measurement. (a) Multiple and (c) single mode-shift of ZnO WGM lasing with a cavity diameter of 5.89 μm under different degrees of bending, (b) multiple and (c) single mode shift of ZnO WGM lasing with a cavity diameter of 4.02 μm under different degrees of bending.

different degrees of bending. Figure 5c is the normalized single lasing mode as the applied tensile strain ranging from 0% to 0.69%, which is extracted from the corresponding lasing spectrum marked with the dashed ellipse in Figure 5a. The obvious redshift of lasing mode has been observed with increasing of tensile strain. The lasing mode with the same order number was distinguished under the tensile strain of 0.51%. Parts b and d of Figure 5 demonstrate the similar redshift tendency of the lasing mode measured in sample #2 as the tensile strain increases from 0% to 0.70%. By applying tensile strain of 0.52%, the lasing mode can be separated thoroughly, which is closed with the results of the two samples mentioned before. Table 2 contrasts the required strain for spectral resolution in two operating type. The strain required to perform the spectral resolution using the lasing-type is 1 order of magnitude smaller than that of PL-type. The lasing-type not only provides an approach for building high-precision and noncontact strain sensor, but also constructs a platform for investigating the piezoelectric field-mediated light and matter interaction in the microcavity.

Table 2. Comparison of the Required Strain for Spectral Resolution in Two Operating Types

type	D (μm)	ΔE (meV)	ε (%)	ref
PL	2.00	~235.00	>3.50	31
	1.10	~280.00	>3.50	
	0.26	~185.00	>3.10	
	0.26	~245.00	>3.50	32
	0.10	~237.50	>7.30	
	5.98	~206.66	~4.47	this work
lasing	5.98	6.64	0.51	this work
	5.89	5.97	0.51	
	4.02	9.26	0.52	

CONCLUSIONS

In conclusion, we developed an approach for dynamically tuning the ZnO WGM lasing wavelength via piezoelectric effect. As a tensile strain is applied, the lasing spectrum is modulated effectively owing to the piezoelectric polarization induced increasing of refractive index. Because of the ultranarrow line width of lasing mode, the sensitivity of strain detection is improved dramatically. In other words, the lasing mode can be distinguished obviously under a tensile strain of 0.51%, while the required strain for spectral resolution in the PL-type operation reaches up to around 4.47% in our case. Our results have not only provided a workable plan for effective modulation of coherent light sources but also proposed an approach for design of high-sensitive flexible optoelectronic micro/nanodevices.

MATERIALS AND METHODS

Sample Preparation. To obtain the high-quality optical microcavity, ZnO microwire arrays were fabricated on the Si substrate by a high-temperature vapor-transport method, as mentioned in our previous report.[43] In brief, a mixture of ZnO and graphite powder with mass ratio of 1:1 was used as the reaction source and filled into a quartz boat coated with a clean Si substrate. Then, it was placed in the center of the heating zone with a reaction temperature of 1050 °C. As reacted lasting for 45 min, ZnO microwire arrays were obtained on the Si substrate. Subsequently, an individual ZnO microwire was picked out and placed on the flexible PET substrate fixed by epoxy resin glue, a mixture of epoxy resin and hardener with mass ratio of 2:1.

Optical Measurement. To characterize the lasing performance of ZnO microwire, a highly integrated microsystem was used (Supporting Information, Figure S1). The frequency-triple 355 nm

DOI: 10.1021/acsnano.8b06500
ACS Nano XXXX, XXX, XXX−XXX

output from a Nd:YAG laser with a repetition rate of 1 kHz and a pulse duration of 50 ns was used as the excitation source and focused on the samples with a 40 μm Gaussian beam spot through an upright microscope (Zeiss M1) equipped with a 10× objective, the emission from ZnO microwire was collected by the same objective and analyzed using a charge-coupled device (CCD) detector and an optical multichannel analyzer (Andor, SR-500i-D1-R) with a 1200 g/mm grating.

ASSOCIATED CONTENT

Supporting Information

The Supporting Information is available free of charge on the ACS Publications website at DOI: 10.1021/acsnano.8b06500.

Optical measurement systems; Raman-shift under tensile strain; strain-dependent PL mapping; Gaussian fitting of NBE emission; analysis of different mode-shift; calculated mode wavelength with decreasing of diameter; experimental mode wavelength under different tensile strain (PDF)

AUTHOR INFORMATION

Corresponding Authors

*Z.L.W.: E-mail, zhong.wang@mse.gatech.edu.
*C.P. E-mail, cfpan@binn.cas.cn.
*C.X.: E-mail, xcxseu@seu.edu.cn

ORCID

Chunxiang Xu: 0000-0001-8116-2869
Caofeng Pan: 0000-0001-6327-9692
Zhong Lin Wang: 0000-0002-5530-0380

Notes

The authors declare no competing financial interest.

ACKNOWLEDGMENTS

We are thankful for the support of the national key R & D project from Minister of Science and Technology, China (2016YFA0202703), National Natural Science Foundation of China (61805015, 51622205, 61675027, 51432005, 61505010, and 51502018), the China Postdoctoral Science Foundation Funded Project (2018M630122), Beijing City Committee of science and technology (Z171100002017019 and Z181100004418004), Beijing Natural Science Foundation (4181004, 4182080, 4184110, and 2184131), and the "Thousand Talents" program of China for pioneering researchers and innovative teams.

REFERENCES

(1) Qian, F.; Li, Y.; Gradečak, S.; Park, H. G.; Dong, Y. J.; Ding, Y.; Wang, Z. L.; Lieber, C. M. Multi-Quantum-Well Nanowire Heterostructures for Wavelength-Controlled Lasers. *Nat. Mater.* **2008**, *7*, 701−706.

(2) Pan, A. L.; Zhou, W. C.; Leong, E. S. P.; Liu, R. B.; Chin, A. H.; Zou, B. S.; Ning, C. Z. Continuous Alloy-Composition Spatial Grading and Superbroad Wavelength-Tunable Nanowire Lasers on a Single Chip. *Nano Lett.* **2009**, *9*, 784−788.

(3) Zong, H.; Yang, Y.; Ma, C.; Feng, X. R.; Wei, T. T.; Yang, W.; Li, J. C.; Li, J. Z.; You, L. P.; Zhang, J.; Li, M.; Pan, C. F.; Hu, X. D.; Shen, B. Flexibly and Repeatedly Modulating Lasing Wavelengths in a Single Core-Shell Semiconductor Microrod. *ACS Nano* **2017**, *11*, 5808−5814.

(4) Yang, Z.; Wang, D. L.; Meng, C.; Wu, Z. M.; Wang, Y.; Ma, Y. G.; Dai, L.; Liu, X. W.; Hasan, T.; Liu, X.; Yang, Q. Broadly Defining Lasing Wavelengths in Single Bandgap-Graded Semiconductor Nanowires. *Nano Lett.* **2014**, *14*, 3153−3159.

(5) Liu, X.; Zhang, Q.; Xiong, Q. H.; Sum, T. C. Tailoring the Lasing Modes in Semiconductor Nanowire Cavities Using Intrinsic Self-Absorption. *Nano Lett.* **2013**, *13*, 1080−1085.

(6) Li, J. B.; Meng, C.; Liu, Y.; Wu, X. Q.; Lu, Y. Z.; Ye, Y.; Dai, L.; Tong, L. M.; Liu, X.; Yang, Q. Wavelength Tunable CdSe Nanowire Lasers Based on the Absorption-Emission-Absorption Process. *Adv. Mater.* **2013**, *25*, 833−837.

(7) Liu, X. F.; Zhang, Q.; Yip, J. N.; Xiong, Q. H.; Sum, T. C. Wavelength Tunable Single Nanowire Lasers Based on Surface Plasmon Polariton Enhanced Burstein-Moss Effect. *Nano Lett.* **2013**, *13*, 5336−5343.

(8) Ma, R. M.; Ota, S.; Li, Y. M.; Yang, S.; Zhang, X. Explosives Detection in a Lasing Plasmon Nanocavity. *Nat. Nanotechnol.* **2014**, *9*, 600−604.

(9) Wang, X. Y.; Wang, Y. L.; Wang, S.; Li, B.; Zhang, X. W.; Dai, L.; Ma, R. M. Lasing Enhanced Surface Plasmon Resonance Sensing. *Nanophotonics* **2017**, *6*, 52−58.

(10) Wang, Z. L. Nanopiezotronics. *Adv. Mater.* **2007**, *19*, 889−892.

(11) Wang, Z. L. Piezopotential Gated Nanowire Devices: Piezotronics and Piezo-Phototronics. *Nano Today* **2010**, *5*, 540−552.

(12) Yang, Q.; Wang, W. H.; Xu, S.; Wang, Z. L. Enhancing Light Emission of ZnO Microwire-Based Diodes by Piezo-Phototronic Effect. *Nano Lett.* **2011**, *11*, 4012−4017.

(13) Yang, Q.; Liu, Y.; Pan, C. F.; Chen, J.; Wen, X. N.; Wang, Z. L. Largely Enhanced Efficiency in ZnO Nanowire/P-Polymer Hybridized Inorganic/Organic Ultraviolet Light-Emitting Diode by Piezo-Phototronic Effect. *Nano Lett.* **2013**, *13*, 607−613.

(14) Kind, H.; Yan, H. Q.; Messer, B.; Law, M.; Yang, P. D. Nanowire Ultraviolet Photodetectors and Optical Switches. *Adv. Mater.* **2002**, *14*, 158−160.

(15) Zhang, F.; Niu, S. M.; Guo, W. X.; Zhu, G.; Liu, Y.; Zhang, X. L.; Wang, Z. L. Piezo-Phototronic Effect Enhanced Visible/UV Photodetector of a Carbon-Fiber/ZnO-CdS Double-Shell Microwire. *ACS Nano* **2013**, *7*, 4537−4544.

(16) Lu, J. F.; Xu, C. X.; Dai, J.; Li, J. T.; Wang, Y. Y.; Lin, Y.; Li, P. L. Improved UV Photoresponse of ZnO Nanorod Arrays by Resonant Coupling with Surface Plasmons of Al Nanoparticles. *Nanoscale* **2015**, *7*, 3396−3403.

(17) Lu, J. F.; Xu, C. X.; Dai, J.; Li, J. T.; Wang, Y. Y.; Lin, Y.; Li, P. L. Plasmon-Enhanced Whispering Gallery Mode Lasing from Hexagonal Al/ZnO Microcavity. *ACS Photonics* **2015**, *2*, 73−77.

(18) Xu, C. X.; Dai, J.; Zhu, G. P.; Zhu, G. Y.; Lin, Y.; Li, J. T.; Shi, Z. L. Whispering-Gallery Mode Lasing in ZnO Microcavities. *Laser Photonics Rev.* **2014**, *8*, 469−494.

(19) Dai, J.; Xu, C. X.; Sun, X. W. ZnO-Microrod/P-GaN Heterostructured Whispering-Gallery-Mode Microlaser Diodes. *Adv. Mater.* **2011**, *23*, 4115−4119.

(20) Lu, J. F.; Jiang, M. M.; Wei, M.; Xu, C. X.; Wang, S. F.; Zhu, Z.; Qin, F. F.; Shi, Z. L.; Pan, C. F. Plasmon-Induced Accelerated Exciton Recombination Dynamics in ZnO/Ag Hybrid Nanolasers. *ACS Photonics* **2017**, *4*, 2419−2424.

(21) Pan, C. F.; Dong, L.; Zhu, G.; Niu, S. M.; Yu, R. M.; Yang, Q.; Liu, Y.; Wang, Z. L. High-Resolution Electroluminescent Imaging of Pressure Distribution Using a Piezoelectric Nanowire LED Array. *Nat. Photonics* **2013**, *7*, 752−758.

(22) Xue, F.; Chen, L. B.; Chen, J.; Liu, J. B.; Wang, L. F.; Chen, M. X.; Pang, Y. K.; Yang, X. N.; Gao, G. Y.; Zhai, J. Y.; Wang, Z. L. P-Type MoS_2 and n-Type ZnO Diode and Its Performance Enhancement by the Piezophototronic Effect. *Adv. Mater.* **2016**, *28*, 3391−3398.

(23) Yang, X.; Dong, L.; Shan, C. X.; Sun, J. L.; Zhang, N.; Wang, S. P.; Jiang, M. M.; Li, B. H.; Xie, X. H.; Shen, D. Z. Piezophototronic-Effect-Enhanced Electrically Pumped Lasing. *Adv. Mater.* **2017**, *29*, 1602832.

(24) Zhou, J.; Gu, Y. D.; Fei, P.; Mai, W. J.; Gao, Y. F.; Yang, R. S.; Bao, G.; Wang, Z. L. Flexible Piezotronic Strain Sensor. *Nano Lett.* **2008**, *8*, 3035−3040.

DOI: 10.1021/acsnano.8b06500
ACS Nano XXXX, XXX, XXX−XXX

(25) Wang, X. D.; Zhou, J.; Song, J. H.; Liu, J.; Xu, N. S.; Wang, Z. L. Piezoelectric Field Effect Transistor and Nanoforce Sensor Based on a Single ZnO Nanowire. *Nano Lett.* **2006**, *6*, 2768−2772.
(26) Li, X. Y.; Liang, R. R.; Tao, J.; Peng, Z. C.; Xu, Q. M.; Han, X.; Wang, X. D.; Wang, C. F.; Zhu, J.; Pan, C. F.; Wang, Z. L. Flexible Light Emission Diode Arrays Made of Transferred Si Microwires-ZnO Nanofilm with Piezo-Phototronic Effect Enhanced Lighting. *ACS Nano* **2017**, *11*, 3883−3889.
(27) Bao, R. R.; Wang, C. F.; Dong, L.; Yu, R. M.; Zhao, K.; Wang, Z. L.; Pan, C. F. Flexible and Controllable Piezo-Phototronic Pressure Mapping Sensor Matrix by ZnO NW/P-Polymer LED Array. *Adv. Funct. Mater.* **2015**, *25*, 2884−2891.
(28) Wang, Z. L.; Song, J. H. Piezoelectric Nanogenerators Based on Zinc Oxide Nanowire Arrays. *Science* **2006**, *312*, 242−246.
(29) Wang, X. D.; Song, J. H.; Liu, J.; Wang, Z. L. Direct-Current Nanogenerator Driven by Ultrasonic Waves. *Science* **2007**, *316*, 102−105.
(30) Signorello, G.; Karg, S.; Björk, M. T.; Gotsmann, B.; Riel, H. Tuning the Light Emission from GaAs Nanowires over 290 meV with Uniaxial Strain. *Nano Lett.* **2013**, *13*, 917−924.
(31) Fu, X. W.; Liao, Z. M.; Liu, R.; Lin, F.; Xu, J.; Zhu, R.; Zhong, W.; Liu, Y. K.; Guo, W. L.; Yu, D. P. Strain Loading Mode Dependent Bandgap Deformation Potential in ZnO Micro/Nanowires. *ACS Nano* **2015**, *9*, 11960−11967.
(32) Wei, B.; Zheng, K.; Ji, Y.; Zhang, Y. F.; Zhang, Z.; Han, X. D. Size-Dependent Bandgap Modulation of ZnO Nanowires by Tensile Strain. *Nano Lett.* **2012**, *12*, 4595−4599.
(33) Han, X. B.; Kou, L. Z.; Lang, X. L.; Xia, J. B.; Wang, N.; Qin, R.; Lu, J.; Xu, J.; Liao, Z. M.; Zhang, X. Z.; Shan, X. D.; Song, X. F.; Gao, J. Y.; Guo, W. L.; Yu, D. P. Electronic and Mechanical Coupling in Bent ZnO Nanowires. *Adv. Mater.* **2009**, *21*, 4937−4941.
(34) Czekalla, C.; Sturm, C.; Schmidt-Grund, R.; Cao, B. Q.; Lorenz, M.; Grundmann, M. Whispering Gallery Mode Lasing in Zinc Oxide Microwires. *Appl. Phys. Lett.* **2008**, *92*, 241102.
(35) Dai, J.; Xu, C. X.; Zheng, K.; Lv, C. G.; Cui, Y. P. Whispering Gallery-Mode Lasing in ZnO Microrods at Room Temperature. *Appl. Phys. Lett.* **2009**, *95*, 241110.
(36) Liu, J. Z.; Lee, S.; Ahn, Y. H.; Park, J. Y.; Koh, K. H.; Park, K. H. Identification of Dispersion-Dependent Hexagonal Cavity Modes of an Individual ZnO Nanonail. *Appl. Phys. Lett.* **2008**, *92*, 263102.
(37) Wiersig, J. Hexagonal Dielectric Resonators and Microcrystal Lasers. *Phys. Rev. A: At., Mol., Opt. Phys.* **2003**, *67*, 023807.
(38) Nobis, T.; Grundmann, M. Low-Order Optical Whispering-Gallery Modes in Hexagonal Nanocavities. *Phys. Rev. A: At., Mol., Opt. Phys.* **2005**, *72*, 063806.
(39) Chen, R.; Ta, V. D.; Sun, H. D. Bending-Induced Bidirectional Tuning of Whispering Gallery Mode Lasing from Flexible Polymer Fibers. *ACS Photonics* **2014**, *1*, 11−16.
(40) Decremps, F.; Pellicer-Porres, J.; Saitta, A. M.; Chervin, J. C.; Polian, A. High-Pressure Raman Spectroscopy Study of Wurtzite ZnO. *Phys. Rev. B: Condens. Matter Mater. Phys.* **2002**, *65*, 092101.
(41) Reparaz, J. S.; Muniz, L. R.; Wagner, M. R.; Goñi, A. R.; Alonso, M. I.; Hoffmann, A.; Meyer, B. K. Reduction of the Transverse Effective Charge of Optical Phonons in ZnO under Pressure. *Appl. Phys. Lett.* **2010**, *96*, 231906.
(42) Vedam, K.; Davis, T. A. Pressure Dependence of the Refractive Indices of the Hexagonal Crystals Beryl, α-CdS, α-ZnS, and ZnO. *Phys. Rev.* **1969**, *181*, 1196−1201.
(43) Lu, J. F.; Li, J. T.; Xu, C. X.; Li, Y.; Dai, J.; Wang, Y. Y.; Lin, Y.; Wang, S. F. Direct Resonant Coupling of Al Surface Plasmon for Ultraviolet Photoluminescence Enhancement of ZnO Microrods. *ACS Appl. Mater. Interfaces* **2014**, *6*, 18301−18305.

DOI: 10.1021/acsnano.8b06500
ACS Nano XXXX, XXX, XXX−XXX